Journal of Electronic Materials (2023) 52:6682–6689
https://doi.org/10.1007/s11664-023-10590-9

ORIGINAL RESEARCH ARTICLE

High Thermoelectric Performance of Large Size $Bi_2Te_{2.7}Se_{0.3}$ Alloy Ingots

Wanwan Zhang[1] · Xin Liu[1] · Zengguo Tian[1] · Yingjiu Zhang[1] · Xin-Jian Li[1] · Hongzhang Song[1]

Received: 23 November 2022 / Accepted: 29 June 2023 / Published online: 25 July 2023

Abstract

Bi_2Te_3-based alloys are currently the best room-temperature thermoelectric materials, and have been used widely in the field of thermoelectric refrigeration. Bi_2Te_3 ingots prepared by the zone-melting method provide convenience for large-scale commercial application. Currently, one trend is that the dimensionless thermoelectric figure-of-merit (*ZT*) value of the *n*-type $Bi_2Te_{2.7}Se_{0.3}$ is slightly lower than that of the *p*-type $Bi_{0.5}Sb_{1.5}Te_3$. In this paper, *n*-type $Bi_2Te_{2.7}Se_{0.3}$ alloy ingots with large size were successfully prepared through the optimized zone-melting preparation process, and achieved a high *ZT* value of 1.16 at 360 K. This value is higher than all the *n*-type or *p*-type Bi_2Te_3-based ingots in current commercial applications.

Keywords Thermoelectric · $Bi_2Te_{2.7}Se_{0.3}$ · large size ingots · commercial applications

Introduction

The ever-increasing population and rapidly developing economy have greatly increased the demand for energy and will inevitably bring about a series of environmental pollution problems. Energy diversification and efficient multi-level utilization have become an effective approach to solve the energy gap without adding additional environmental burdens.[1,2] Thermoelectric materials can realize the direct conversion between thermal energy and electric energy.[3] For example, it can convert a large amount of waste heat and residual heat which are difficult to utilize in industry into electric energy[4], and has attracted extensive attention from industry and academia.[5] Thermoelectric materials are mainly used in the fields of thermoelectric power generation and thermoelectric cooling.[6] Due to their irreplaceable advantages and characteristics, such as adaptability, diversity, and reliability, thermoelectric materials are receiving unprecedented expectations as the key technology supporting many modern industries.[7–9]

The conversion efficiency of a thermoelectric material is characterized by its dimensionless thermoelectric figure-of-merit (*ZT*) value. The *ZT* value is closely related to mainly physical quantities, such as resistivity (ρ), Seebeck coefficient (S), thermal conductivity (κ), and absolute temperature (T). The specific relationship is $ZT = \frac{S^2}{\rho\kappa}T$. The thermoelectric properties are divided into two parts: electrical transport properties and thermal transport properties. The electrical transport properties can be characterized by the power factor $\left(PF = \frac{S^2}{\rho}\right)$. Good electrical conductivity is one of the characteristics of thermoelectric materials, so most of the research on thermoelectric materials initially focused on metals and their alloys with extremely low resistivity. However, it was later discovered that the Seebeck coefficient of metallic materials is too small. Metallic materials are not destined to be excellent thermoelectric materials. With the development of semiconductor materials, thermoelectric materials have again become a research boom and rapidly entered an explosive stage.[10–13] In the 1950s, Bi_2Te_3-based thermoelectric materials quickly became the focus of researchers as soon as they were discovered, and entire research was centered on how to obtain high *ZT* values.[14] In the following decades, Bi_2Te_3-based thermoelectric materials continued to refresh the highest *ZT* values.[15–17] Bi_2Te_3 is a typical narrow-band semiconductor material.[18] It has a high density of states and effective electronic mass due to its complex energy band structure. Furthermore, because of the small electronegativity difference between Bi and Te atoms, it helps to obtain higher carrier mobility.

✉ Hongzhang Song
hzsong@zzu.edu.cn

[1] Key Laboratory of Material Physics of Ministry of Education, School of Physics and Microelectronics, Zhengzhou University, Zhengzhou 450001, China

Under the influence of multiple factors, Bi_2Te_3 alloys became the optimal thermoelectric material systems near room temperature.[15,19]

Furthermore, Bi_2Te_3 thermoelectric materials are currently the only thermoelectric material system widely used in business, such as refrigeration near room temperature.[20–22] However, the *ZT* value of commercial Bi_2Te_3 is mostly below 0.9. The development of high-performance Bi_2Te_3 thermoelectric materials is conducive to further seize the thermoelectric material market. On the whole, the performance of *n*-type materials is not yet comparable to that of *p*-type materials.[4,23–27] Therefore, the research and development of high-performance *n*-type $Bi_2Te_{2.7}Se_{0.3}$ alloys is more important. The common preparation methods of thermoelectric materials include hot pressing (HP),[28,29] spark plasma sintering (SPS),[30,31] zone melting,[32,33] etc. The *ZT* values of $Bi_2Te_{2.7}Se_{0.3}$ thermoelectric materials prepared by different methods are not the same.[34] In this paper, the zone-melting method was used to prepare *n*-type $Bi_2Te_{2.7}Se_{0.3}$ crystals. Compared with other preparation methods, its products have a large size and higher thermoelectric properties due to texturing, which is beneficial for commercial applications. Especially, compared to the conventional zone-melting process, the zone-melting method in this paper was optimized by using quartz tubes instead of common glass tubes, and two vacuum pumps instead of one mechanical pump, and adding a process of swing furnace.

Experimental

All samples in this experiment were prepared using the zone-melting method. The *n*-type $Bi_2Te_{2.7}Se_{0.3}$ ingredients were weighed according to the stoichiometric ratio, mixed, and sealed in a high-vacuum quartz tube. In the swing furnace, the raw materials were shaken for 10 h at 1023 K to achieve the effect of uniform mixing of the ingredients. Cooled to room temperature, the quartz tube was fixed on a zone fusion furnace. The melted ingot underwent zone fusion crystal growth at a temperature of 973 K with a growing rate of 8 mm/h. After the zone-melting temperature dropped to room temperature, the *n*-type $Bi_2Te_{2.7}Se_{0.3}$ ingot were removed from the broken quartz tube. The ingot was cut into the required size for testing the electrical and thermal properties using a wire-cut electrical discharge machining. The sample size for electrical performance testing was 2 mm × 3 mm × 13 mm, and the sample size for thermal performance testing was 2 mm × 10 mm × 10 mm.

The treated samples were subjected to various microstructure characterization and performance tests. The phase structure of the material was characterized by an x-ray diffraction analyzer (XRD), and the micromorphology was observed by scanning electron microscopy (SEM). Regarding thermoelectric performance, this mainly includes two aspects: electrical transport performance (Seebeck coefficient and resistivity) and thermal transport performance (thermal conductivity). The LSR system (LSR-3/800 Seebeck coefficients/electrical resistance measuring system; Linseis, Germany) can simultaneously measure the Seebeck coefficient and the resistivity of the sample. The inert gas environment during the test was provided by argon. The thermal conductivity was calculated by the formula $\kappa = dDC_p$. The physical symbols d, D , and C_p represent the density, thermal diffusion coefficient, and specific heat capacity of the material, respectively. They were calculated using the Archimedes principle, tested by the LFA457 system (Netzsch, Germany), and measured by differential scanning calorimetry (DSC) independently.

Results and Discussion

The $Bi_2Te_{2.7}Se_{0.3}$ alloy in this paper has two distinct advantages. The first is that the thermoelectric properties are generally higher than those of the $Bi_2Te_{2.7}Se_{0.3}$ currently on the market. The second is that $Bi_2Te_{2.7}Se_{0.3}$ can be produced at large scale to meet the needs of commercialization. The ingot length was 28 cm and its diameter was 2.6 cm, as shown in Fig. 1. In order to obtain more reliable data, three sets of samples taken from different areas of the ingot (Fig. 1) were tested separately for thermoelectric performance. In addition, the thermoelectric properties were tested along two different directions, one parallel to the zone melting direction (results are shown in Fig. 3), and the other perpendicular to the zone-melting direction.

Figure 2 shows the XRD pattern for the $Bi_2Te_{2.7}Se_{0.3}$ ingot. By comparing the standard cards and several published reports, the diffraction peaks of this group of samples match well, with no impurity diffraction peaks, confirming that this group of samples is the target material.

In Fig. 3a, the resistivity of all the samples is proportional to temperature, exhibiting typical degenerate semiconductor characteristics. In Fig. 3b, the Seebeck coefficient of all the samples is negative, indicating that the samples are all

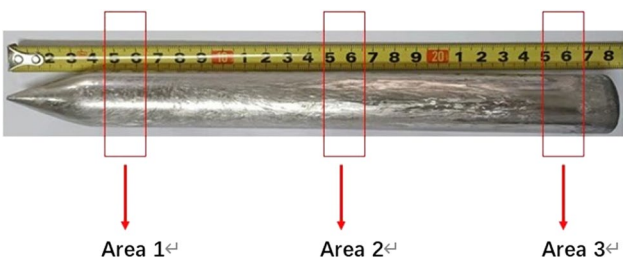

Fig. 1 The $Bi_2Te_{2.7}Se_{0.3}$ ingot; the red box refers to the area of the sample (Color figure online).

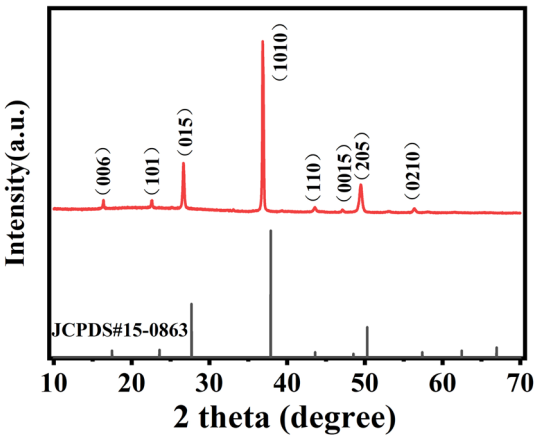

Fig. 2 XRD patterns for the $Bi_2Te_{2.7}Se_{0.3}$ ingot.

n-type semiconductors with electrons as the main carrier. The Seebeck coefficient gradually increases with increasing temperature, reaching its maximum value at a certain temperature, and then begins to decrease. This phenomenon is attributed to the bipolar effect. At higher temperatures, due to the intrinsic thermal excitation, electron and hole pairs are produced in thermoelectric materials, while due to the opposite sign of the Seebeck coefficients of the electrons and holes, the minority carrier would decrease the Seebeck coefficient. Thus an *S* peak appears. The highest values of the Seebeck coefficient for the *n*-type $Bi_2Te_{2.7}Se_{0.3}$ sample prepared by hot pressing were about 140–160 $\mu V/K$.[35] The absolute value of the Seebeck coefficient of the *n*-type $Bi_2Te_{2.7}Se_{0.3}$ sample prepared by SPS is below 200 $\mu V/K$,[36,37] but the absolute value of the Seebeck coefficient in this experiment is 205–230 $\mu V/K$. Compared with other experimental methods, the *ZT* values of the $Bi_2Te_{2.7}Se_{0.3}$ samples in this study may be not the highest, but their high Seebeck values make them more competitive because of their high detection sensitivity. The power factor calculated by the resistivity and the Seebeck coefficient is shown in Fig. 3c. The highest power factor can be achieved near room temperature.

The physical quantity that characterizes the thermal transport properties of materials is the thermal conductivity (κ). This is composed of three parts: electronic thermal conductivity, lattice thermal conductivity, and bipolar thermal conductivity. There is a strong correlation between the electronic thermal conductivity and the electrical resistivity. Low resistance and large electronic thermal conductivity always occur together. So, the electronic thermal conductivity is not easy to individually control. The lattice thermal conductivity is a relatively independent parameter, and research on thermal conductivity generally focuses on reducing the lattice thermal conductivity.[38–40] In the $Bi_2Te_{2.7}Se_{0.3}$ materials, both Bi and Te atoms have large atomic masses, and the melting point of the system is lower (about 858 K), so the system has a lower lattice thermal conductivity, as shown in Fig. 3d. In Fig. 3e, the total thermal conductivity first decreases due to the enhanced phonon scattering, and then increases with increasing temperature due to the bipolar effect. It changes in the range of 1.3–1.7 $W/m.K$.

Under the combined effect of the Seebeck coefficient, resistivity, and thermal conductivity, the *ZT* of the material first increases and then decreases with temperature, as shown in Fig. 3f. In the temperature range of 300–400 K, *ZT* values of more than 1 are achieved. At 360 K, the *n*-type $Bi_2Te_{2.7}Se_{0.3}$ obtains an optimum *ZT* value as high as 1.16. This value may be lower than some reported values whose bulk samples are prepared by HP, SPS, HTHP, LSM, etc., [4,25,26,41–50] is a highly competitive one in the zone-melting field due to the high vacuum, high pure raw materials, and swing sintering in this experiment.[32,33,51] In particular, four Bi_2Te_3-based alloy ingots can be simultaneously prepared in the zone-melting furnace. So, the preparation process in this paper can be directly industrialized.

On the whole, the three groups of samples show similar patterns, but the performance of the area 2 sample is better than the other two samples. This is because the areas 1 and 3 are located at the two ends of the ingot, respectively. The samples in these two areas are prone to component segregation during the zone-melting process, which reduces the thermoelectric properties. That is to say, some samples with poor performance may be produced at the two ends of the ingot, while the size of the two specific areas needs to be further studied.

The samples prepared by zone melting are polycrystalline with oriented growth characteristics, and their mechanical properties are better than those of single crystals. Element doping was used to adjust the carrier concentration to achieve a uniform distribution of impurities, and the thermoelectric performance is then more stable. Figure 4 shows the fracture morphology of the $Bi_2Te_{2.7}Se_{0.3}$ sample. The observed directions in Fig. 4a and b are parallel and perpendicular to the zone-melting direction, respectively. The morphology is a typical layered density structure. The test results of the thermoelectric properties of the $Bi_2Te_{2.7}Se_{0.3}$ sample taken from area 2 along two directions are shown in Fig. 5.

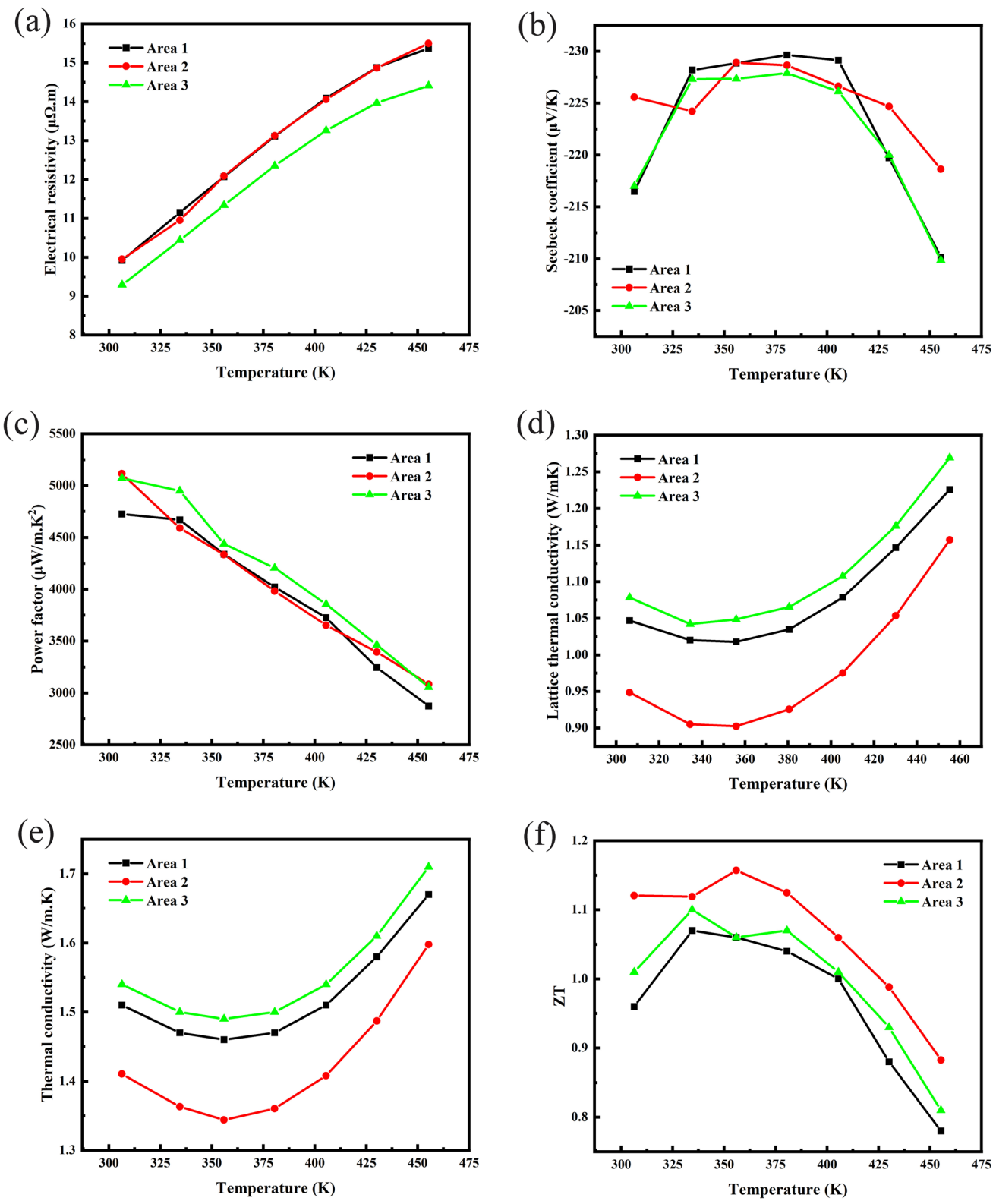

Fig. 3 Variation of thermoelectric properties with temperature for different regions of $Bi_2Te_{2.7}Se_{0.3}$: (a) resistivity, (b) Seebeck coefficients, (c) power factors, (d) lattice thermal conductivity, (e) total thermal conductivity, and (f) *ZT* values.

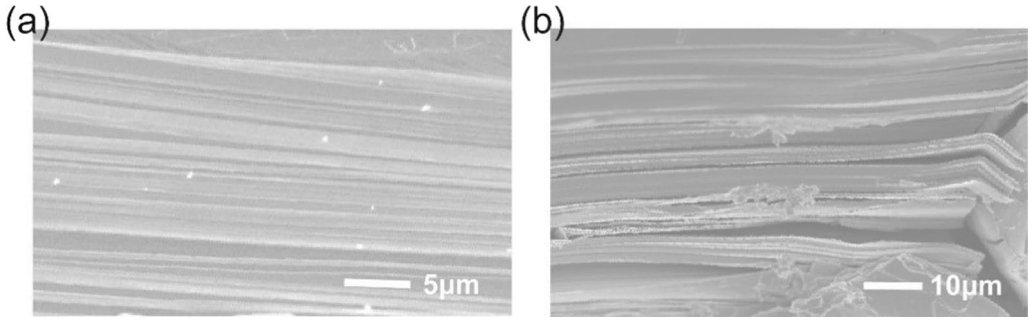

Fig. 4 SEM fracture morphology diagram of $Bi_2Te_{2.7}Se_{0.3}$ along two tested directions: (a) parallel to the zone melting direction, (b) perpendicular to the zone melting direction.

Figure 5a shows the change trend of the sample's resistivity with temperature in two directions. The resistivity increases with increasing temperature, differs significantly in the two directions and has obvious anisotropy. The numerical ratio of the resistivity in the two directions is called the anisotropy ratio of resistivity.[40] In this experiment, the electrical resistivity perpendicular and parallel to the zone-melting directions at room temperature was 17.66 $\mu\Omega.m$ and 9.95 $\mu\Omega.m$, respectively. The calculated anisotropy ratio was 1.78, which is lower or comparable to the data in the literature.[33,52] This anisotropy of electrical conductivity in the *n*-type $Bi_2Te_{2.7}Se_{0.3}$ ingot is well understood by the anisotropic nature in carrier mobility as the crystallographic directions, as demonstrated by its texturing and layered microstructure shown in Figs. 1 and 4. Figure 5b shows the variation range of the Seebeck coefficient in two directions. Within the experimental error range, the experimental data in the two directions are roughly the same. In other words, the Seebeck coefficient is isotropic.[53] This is consistent with the theoretical calculation results based on the relaxation time approximation.[54] Through the above analysis, the samples with parallel zone-melting directions have a high Seebeck coefficient and low resistivity at the same time. The sample in the parallel zone-melting direction has a higher power factor, which is about 1.9 times that of the perpendicular zone-melting direction. Their power factors calculated by resistivity and Seebeck coefficient are shown in Fig. 5c.

The lattice thermal conductivity and the total thermal conductivity of $Bi_2Te_{2.7}Se_{0.3}$ ingot in two directions varies with temperature, as shown in Fig. 5d and e, respectively. The test results indicate that the total thermal conductivity in the parallel zone melting direction is 1.41 $W/m.K$ near room temperature, which is larger than that in the perpendicular zone melting direction of 0.9 $W/m.K$. This is because the preferred orientation of the sample favors the heat transport of carriers and phonons along the crystal plane. The anisotropic ratio of thermal conductivity is 1.56, which is much smaller than the value of the single crystal sample (2.1–2.4) as well as smaller than the textured $Bi_2Te_2Se_1$ bulk sample.[55,56]

Figure 5f shows the *ZT* value obtained by calculation. The Seebeck coefficient of the $Bi_2Te_{2.7}Se_{0.3}$ sample prepared by zone melting is isotropic, and the thermal conductivity and resistivity have different degrees of anisotropy. Since the resistivity ratio of the two directions is greater than the thermal conductivity ratio, the *ZT* value of the material shows that the parallel zone-melting direction is better than the perpendicular zone-melting direction. This is the same as the conclusion of Wang et al.[57]

Conclusions

The emergence of thermoelectric materials provides new ideas for solving the energy crisis and environmental pollution.[58–64] As typical excellent room-temperature thermoelectric materials, $Bi_2Te_{2.7}Se_{0.3}$ alloys have successfully achieved commercial applications. However, the current commercial $Bi_2Te_{2.7}Se_{0.3}$ alloys have low *ZT* values. The $Bi_2Te_{2.7}Se_{0.3}$ sample in this article has achieved a *ZT* value of more than 1.0 near room temperature, and the highest value can reach 1.16. The ingot size is large, which improves its utilization. By testing the thermoelectric properties in different directions, it is confirmed that the $Bi_2Te_{2.7}Se_{0.3}$ ingot has anisotropy, and that the thermoelectric properties in the

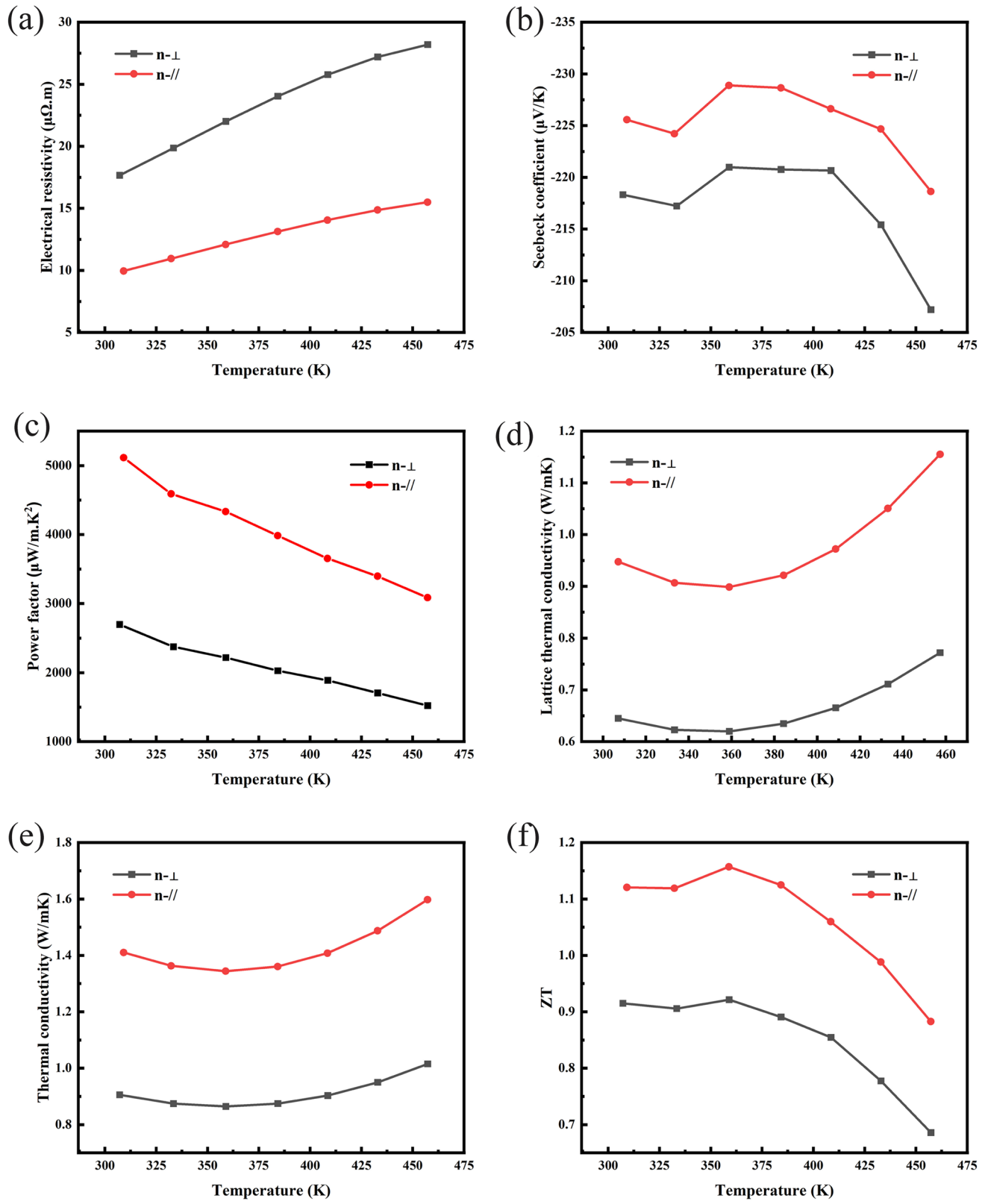

Fig. 5 Variation of thermoelectric properties of $Bi_2Te_{2.7}Se_{0.3}$ with temperature along the two tested directions: (a) resistivity, (b) Seebeck coefficients, (c) power factors, (d) lattice thermal conductivity, (e) total thermal conductivity, and (f) *ZT* values; *N*-⊥perpendicular to the zone-melting direction, *N*-// parallel to the zone melting direction.

parallel zone-melting direction are greatly improved, which is consistent with the results in the literature.

Conflict of interest There are no conflicts to declare.

Data availability Data will be made available on reasonable request.

References

1. Y. Wang, Y.V. Lim, S. Huang, M. Ding, D. Kong, Y. Pei, T. Xu, Y. Shi, X. Li, and H.Y. Yang, Enhanced sodium storage kinetics by volume regulation and surface engineering via rationally designed hierarchical porous FeP@ C/rGO. *Nanoscale* 12, 4341 (2020).
2. X. Li, J. Fu, Y. Sun, M. Sun, S. Cheng, K. Chen, X. Yang, Q. Lou, T. Xu, Y. Shang, J. Xu, Q. Chen, and C. Shan, Design and understanding of core/branch-structured VS_2 nanosheets@CNTs as high-performance anode materials for lithium-ion batteries. *Nanoscale* 11, 13343 (2019).
3. M. Shen, S. Lu, Z. Zhang, H. Liu, and X. Jia, Bi and Sn Co-doping enhanced thermoelectric properties of Cu_3SbS_4 materials with excellent thermal stability. *ACS Appl. Mater. Inter.* 12, 8271 (2020).
4. B. Zhu, X. Liu, Q. Wang, Y. Qiu, Z. Shu, Z. Guo, Y. Tong, J. Cui, M. Gu, and J. He, Realizing record high performance in *n*-type Bi_2Te_3-based thermoelectric materials. *Energy Environ. Sci.* 13, 2106 (2020).
5. M. Hong, Z.-G. Chen, L. Yang, Y.C. Zou, and J. Zou, Realizing zT of 2.3 in $Ge_{1-x-y}Sb_xIn_yTe$ via reducing the phase-transition temperature and introducing resonant energy doping. *Adv. Mater.* 30, 1705942 (2018).
6. Z. Zhu, Y. Zhang, H. Song, and X.-J. Li, Enhancement of thermoelectric performance of $Cu_{1.98}Se$ by Pb doping. *Appl. Phys. A* 124, 747 (2018).
7. Y. Yu, C. Zhou, S. Zhang, M. Zhu, M. Wuttig, C. Scheu, D. Raabe, G.J. Snyder, B. Gault, and O. Cojocaru-Mirédin, Revealing nano-chemistry at lattice defects in thermoelectric materials using atom probe tomography. *Mater. Today* 32, 260 (2020).
8. C.B. Vining, Semiconductors are cool. *Nature* 413, 577 (2001).
9. J. He and T.M. Tritt, Advances in thermoelectric materials research: looking back and moving forward. *Science* 357, 1369 (2017).
10. H.J. Goldsmid and R.W. Douglas, The use of semiconductors in thermoelectric refrigeration. *Br. J. Appl. Phys.* 5, 386 (1954).
11. H. Qin, L. Xie, Z. Zhang, D. Qin, F. Guo, W. Cai, Q. Zhang, and J. Sui, Rare earth ytterbium enhanced thermoelectric properties of p-type $Bi_{0.5}Sb_{1.5}Te_3$. *Appl. Phys. Lett.* 114, 123901 (2019).
12. S. Kim, K.H.G. Lee, H.A. Mun, H.S. Kim, S.W. Hwang, J.W. Roh, D.J. Yang, W.H. Shin, X.S. Li, and Y.H. Lee, Dense dislocation arrays embedded in grain boundaries for high-performance bulk thermoelectrics. *Science* 348, 109 (2015).
13. L. Hu, T. Zhu, X. Liu, and X. Zhao, High performance n-type bismuth telluride based alloys for mid-temperature power generation. *Adv. Funct. Mater.* 24, 5211 (2015).
14. F. Wu, Q. He, M. Tang, and H. Song, Thermoelectric properties of Tl and I dual-doped Bi_2Te_3 based alloys. *Int. J. Mod. Phys. B* 32, 1850123 (2018).
15. I. Malik, T. Srivastava, K.K. Surthi, C. Gayner, and K.K. Kar, Enhanced thermoelectric performance of n-type Bi_2Te_3 alloyed with low cost and highly abundant sulfur. *Mater. Chem. Phys.* 255, 123598 (2020).
16. J.P. Heremans, R.J. Cava, and N. Samarth, Tetradymites as thermoelectrics and topological insulators. *Nat. Rev. Mater.* 2, 17049 (2017).
17. H. Cho, J.H. Yun, H.K. Jin, Y.B. Song, and J.S. Rhyee, Possible charge density wave and enhancement of thermoelectric properties at mild-temperature range in n-type CuI-doped $Bi_2Te_{2.1}Se_{0.9}$ compounds. *ACS Appl. Mater. Inter.* 12, 925 (2019).
18. H. Xie, X. Su, G. Zheng, T. Zhu, K. Yin, Y. Yan, C. Uher, M.G. Kanatzidis, and X. Tang, The role of Zn in chalcopyrite $CuFeS_2$: enhanced thermoelectric properties of $Cu_{1-x}Zn_xFeS_2$ with in situ nanoprecipitates. *Adv. Energy Mater.* 7, 1601299 (2017).
19. J.J. Shen, T.J. Zhu, X.B. Zhao, S.N. Zhang, S.H. Yang, and Z.Z. Yin, Recrystallization induced in situ nanostructures in bulk bismuth antimony tellurides: a simple top down route and improved thermoelectric properties. *Energy Environ. Sci.* 3, 1519 (2010).
20. L. Hu, T. Zhu, X. Liu, and X. Zhao, Point defect engineering of high-performance bismuth-telluride-based thermoelectric materials. *Adv. Funct. Mater.* 24, 5211 (2014).
21. D. Li, J.M. Li, J.C. Li, Y.S. Wang, and G.D. Tang, High thermoelectric performance of n-type $Bi_2Te_{2.7}Se_{0.3}$ via nanostructure engineering. *J. Mater. Chem. A* 6, 9642 (2018).
22. Z. Huang, S. Li, R. Wang, C. Wang, W. Zhao, N. Yang, F. Liu, J. Luo, Y. Xiao, and F. Pan, Precision grain boundary engineering in commercial $Bi2Te_{2.7}Se_{0.3}$ thermoelectric materials towards high performance. *J. Mater. Chem. A* 9, 11442 (2021).
23. Y. Zhou, F. Meng, J. He, A. Benton, L. Hu, F. Liu, J. Li, Ch. Zhang, W. Ao, and H. Xie, n-$Bi_{2-x}Sb_xTe_3$: a promising alternative to mainstream thermoelectric material n-Bi_2Te_3–xSe_x near room temperature. *ACS Appl. Mater. Inter.* 12, 31619 (2020).
24. R. Cao, X. Liu, Z. Tian, Y. Zhang, X.-J. Li, and H. Song, Improving the thermoelectric properties of $Bi2Te_{2.7}Se_{0.3}$ through La2O3 dispersion. *Appl. Phys. A* 128, 1130 (2022).
25. J. Yang, F. Wu, Z. Zhu, L. Yao, H. Song, and X. Hu, Thermoelectrical properties of lutetium-doped Bi_2Te_3bulk samples prepared from flower-like nanopowders. *J. Alloys Compd.* 619, 401 (2015).
26. Q. Hu, W. Qiu, L. Chen, J. Chen, L. Yang, and J. Tang, Realize high thermoelectric properties in *n*-Type $Bi_2Te_{2.7}Se_{0.3}/Y_2O_3$ nanocomposites by constructing heterointerfaces. *ACS Appl. Mater. Inter.* 13, 38526 (2021).
27. Q. Zhang, X. Lu, J. Liao, H. Chen, Y. Fan, J. Xing, S. Gu, J. Huang, J. Ma, J. Wang, L. Wang, and W. Jiang, High-efficiency thermoelectric power generation enabled by homogeneous incorporation of MXene in (Bi, $Sb_)2T_e3$ Matrix. *Adv. Energy Mater.* 10, 1902986 (2020).
28. R.-S. Zhai, Y.-H. Wu, T.-J. Zhu, and X.-B. Zhao, Thermoelectric performance of *p*-type zone-melted Se-doped $Bi_{0.5}Sb_{1.5}Te_3$ alloys. *Rare Metals* 37, 308 (2018).
29. Q. He, W. Zhang, X. Liu, and H. Song, Enhanced thermoelectric performance of Bi_2Te_3 by La_2O_3 dispersion. *Mod. Phys. Lett. B* 36, 2250157 (2022).
30. X.L. Shi, J. Zou, and Z.-G. Chen, Advanced thermoelectric design: from materials and structures to devices. *Chem. Rev.* 120, 7399 (2020).
31. C.J. Vineis, A. Shakouri, A. Majumdar, and M.G. Kanatzidis, Nanostructured thermoelectrics: big efficiency gains from small features. *Adv. Mater.* 22, 3970 (2010).
32. K.F. Hsu, S. Loo, F. Guo, W. Chen, J.S. Dyck, C. Uher, T. Hogan, E.K. Polychroniadis, and M.G. Kanatzidis, Cubic $AgPbmSbTe_{2+m}$: bulk thermoelectric materials with high figure of merit. *Science* 303, 818 (2004).
33. L. Chen, Z. Guo, Q. Zhang, G. Wu, X. Tan, Y. Yin, H. Hu, G. Liu, and J. Jiang, Optimized thermoelectric properties of $Bi_{0.48}Sb_{1.52}$Te3/BN composites. *J. Mater. Chem. C* 10, 3172 (2022).

34. Y. Pan, U. Aydemir, F.H. Sun, C.F. Wu, and J.F. Li, Self-Tuning *n*-type Bi_2(Te, Se_3)3/SiC thermoelectric nanocomposites to realize high performances up to 300 °C. *Adv. Sci.* 4, 1700259 (2017).
35. R. Cao, H. Song, W. Gao, E. Li, X. Li, and X. Hu, Thermoelectric properties of Lu-doped n-type $Lu_xBi_{2-x}Te_{2.7}Se_{0.3}$ alloys. *J. Alloys Compd.* 727, 326 (2017).
36. Y. Pan and J.F. Li, Thermoelectric performance enhancement in *n*-type $Bi_2(TeSe)_3$ alloys owing to nanoscale inhomogeneity combined with a spark plasma-textured microstructure. *NPG Asia Mater.* 8, 275 (2016).
37. J.Y. Hwang, S. Choi, S. Kim, J.H. Lim, and K.H. Lee, Hf-doping effect on the thermoelectric transport properties of *n*-type $Cu_{0.01}Bi_2Te_{2.7}Se_{0.3}$. *Appl. Sci.* 10, 4875 (2020).
38. R. Deng, X. Su, S. Hao, Z. Zheng, M. Zhang, H. Xie, W. Liu, Y. Yan, C. Wolverton, and C. Uher, High thermoelectric performance in Bi0 $46Sb_{1.54}Te_3$ nanostructured with ZnTe. *Energy Environ. Sci.* 11, 1520 (2018).
39. Y. Zhu, B. Wan, W. Shen, Z. Zhang, C. Fang, Q. Wang, L. Chen, Y. Zhang, and X. Jia, Controllable 2H/3R phase transition and conduction behavior change in $MoSe_2$: Nb substitution by high pressure synthesis for promising thermoelectric conversion. *Appl. Phys. Lett.* 122, 133903 (2023).
40. W.M. Yim, E.V. Fitzke, and F.D. Rosi, Thermoelectric properties of Bi_2Te_3-Sb_2Te_3-Sb_2Se_3 pseudo-ternary alloys in the temperature range 77 to 300°K. *J. Mater. Sci.* 1, 52 (1966).
41. X. Liu, R. Cao, Y. Zhang, Z. Tian, X.-J. Li, and H. Song, Excellent dispersion effects of carbon nanodots on the thermoelectric properties of $Bi_2Te_{2.7}Se_{0.3}$ with excessive Te. *J. Alloys Compd.* 899, 163296 (2022).
42. R. Cao, Z. Zhu, X.-J. Li, X. Hu, and H. Song, Enhanced thermoelectric properties of the Lu-doped and CNT dispersed Bi_2Te_3 alloy. *Appl. Phys. A* 125, 126 (2019).
43. Y. Zhang, X. Jia, L. Deng, X. Guo, H. Sun, B. Sun, B. Liu, and H. Ma, Evolution of thermoelectric properties and anisotropic features of Bi_2Te_3 prepared by high pressure and high temperature. *J. Alloys Compd.* 632, 514 (2015).
44. L. Hu, H. Wu, T. Zhu, C. Fu, J. He, P. Ying, and X. Zhao, Tuning multiscale microstructures to enhance thermoelectric performance of n-type Bismuth-Telluride-based solid solutions. *Adv. Energy Mater.* 5, 1500411 (2015).
45. F. Wu, H. Song, J. Jia, F. Gao, Y. Zhang, and X. Hu, Thermoelectric properties of Ce-doped *n*-type $Ce_xBi_{2-x}Te_{2.7}Se_{0.3}$ nanocomposites. *Phys. Status Solidi A* 210, 1183 (2013).
46. B. Zhu, Z.-Y. Huang, X.-Y. Wang, Y. Yu, L. Yang, N. Gao, Z.-G. Chen, and F.-Q. Zu, Attaining ultrahigh thermoelectric performance of direction-solidified bulk n-type $Bi_2Te_{2.4}Se_{0.6}$ via its liquid state treatment. *Nano Energy* 42, 8 (2017).
47. L. Hu, Y. Zhang, H. Wu, Y. Liu, J. Li, J. He, W. Ao, F. Liu, S.J. Pennycook, and X. Zeng, Synergistic compositional–mechanical–thermal effects leading to a record high zT in *n*-type V_2VI_3 alloys through progressive hot deformation. *Adv. Funct. Mater.* 28, 1803617 (2018).
48. Y. Wu, Y. Yu, Q. Zhang, T. Zhu, R. Zhai, and X. Zhao, Liquid-phase hot deformation to enhance thermoelectric performance of *n*-type bismuth-telluride-based solid solutions. *Adv. Sci.* 6, 1901702 (2019).
49. B. Jabar, X. Qin, A. Mansoor, H. Ming, L. Huang, M.H. Danish, J. Zhang, D. Li, C. Zhu, H. Xin, and C. Song, Enhanced power factor and thermoelectric performance for *n*-type $Bi_2Te_{2.7}Se_{0.3}$ based composites incorporated with 3D topological insulator nanoinclusions. *Nano Energy* 80, 105512 (2021).
50. C.-H. Lin, W.-T. Yen, Y.-F. Tsai, and H.-J. Wu, Unravelling p–n conduction transition in high thermoelectric figure of merit gallium-doped Bi_2Te_3 via phase diagram engineering. *ACS Appl. Energy Mater.* 3, 1311 (2020).
51. J. Pei, B. Cai, H.L. Zhuang, and J.-F. Li, Bi_2Te_3-based applied thermoelectric materials: research advances and new challenges. *Nat. Sci. Rev.* 7, 1856 (2020).
52. O. Ben-Yehuda, R. Shuker, Y. Gelbstein, Z. Dashevsky, and M.P. Dariel, Highly textured Bi_2Te_3-based materials for thermoelectric energy conversion. *J. Appl. Phys.* 101, 113707 (2007).
53. H. Huang, J. Li, S. Chen, Z. Zhang, Y. Yan, X. Su, and X. Tang, Anisotropic thermoelectric transport properties of $Bi_{0.5}Sb_{1.5}Te^2$ 96+x zone melted ingots. *J. Solid State Chem.* 288, 121433 (2020).
54. W.E. Bies, R.J. Radtke, and H. Ehrenreich, Thermoelectric properties of anisotropic semiconductors. *Phys. Rev. B* 65, 85208 (2002).
55. M. Carle, C. Lahallegravier, S. Scherrer, H. Scherrer, and P. Pierrat, Transport properties of n-type $Bi_2(Te_{1-x}Se_x)_3$ single crystal solid solutions (x≤0.05). *J. Phys. Chem. Solids* 56, 201 (1995).
56. L.P. Hu, X.H. Liu, H.H. Xie, J.J. Shen, T.J. Zhu, and X.B. Zhao, Improving thermoelectric properties of n-type bismuth–telluride-based alloys by deformation-induced lattice defects and texture enhancement. *Acta Mater.* 60, 4431 (2012).
57. M. Wang, Z. Tang, T. Zhu, and X.B. Zhao, The effect of texture degree on the anisotropic thermoelectric properties of (Bi, $Sb)_2$(Te, $Se)_3$ based solid solutions. *RSC Adv.* 6, 98646 (2016).
58. W.-Y. Chen, X.L. Shi, J. Zou, and Z.-G. Chen, Thermoelectric coolers for on-chip thermal management: materials, design, and optimization. *Mater. Sci. Eng. R* 151, 100700 (2022).
59. R. Ma, D. Yang, Z. Tian, H. Song, and Y. Zhang, Effects of Bi_2Te_3 doping on the thermoelectric properties of Cu_2Se alloys. *Appl. Phys. A* 128, 531 (2022).
60. Z. Zhu, Y. Zhang, H. Song, and X.-J. Li, High thermoelectric performance and low thermal conductivity in $Cu_{2-x}Na_xSe$ bulk materials with micro-pores. *Appl. Phys. A* 125, 572 (2019).
61. R. Cao, E. Li, Q. Hu, Z. Zhu, Y. Zhang, X. Li, X. Hu, and H. Song, Enhanced thermoelectric properties of $Cu_{2-\delta}Se$ nanopowder dispersed $Bi_2Ba_2Co_2O_y$ ceramics. *Appl. Phys. A* 124, 669 (2018).
62. R. Ma, D. Yang, Z. Tian, H. Song, and Y. Zhang, Thermoelectric properties in nano Y_2O_3 dispersed Cu_2Se. *Appl. Phys. A* 128, 1134 (2022).
63. L. Su, D. Wang, S. Wang, B. Qin, Y. Wang, Y. You, Y. Yin, C. Chang, and L.-D. Zhao, High thermoelectric performance realized through manipulating layered phonon-electron decoupling. *Science* 375, 1385 (2022).
64. S. Xia, H. Song, S. Liu, and H. Hao, Low thermal conductivity and thermoelectric properties of $Si_{80}Ge_{20}$ dispersed $Bi_2Sr_2Co_2O_y$ ceramics. *Ceram. Int.* 49, 4707 (2023).